Molecular Insights into the Intrinsic Dynamics and Their Roles During Catalysis in Pin1 Peptidyl-prolyl Isomerase

Mori, Toshifumi
Institute for Materials Chemistry and Engineering, Kyushu University

Saito, Shinji
Institute for Molecular Science

出版情報：Journal of Physical Chemistry B. 126 (28), pp.5185-5193, 2022-07-21. American Chemical Society
バージョン：

Molecular Insights into the Intrinsic Dynamics and Their Roles During Catalysis in Pin1 Peptidyl-prolyl Isomerase

Toshifumi Mori*,†,‡ and Shinji Saito*,¶,§

†*Institute for Materials Chemistry and Engineering, Kyushu University, Kasuga, Fukuoka 816-8580, Japan*

‡*Department of Interdisciplinary Engineering Sciences, Interdisciplinary Graduate School of Engineering Sciences, Kyushu University, Kasuga, Fukuoka 816-8580, Japan*

¶*Institute for Molecular Science, Myodaiji, Okazaki, Aichi, 444-8585, Japan*

§*School of Physical Sciences, The Graduate University for Advanced Studies, Okazaki, Aichi 444-8585, Japan*

E-mail: toshi_mori@cm.kyushu-u.ac.jp; shinji@ims.ac.jp

Abstract

Proteins are intrinsically dynamic and change conformations over a wide range of timescales. While the conformational dynamics have been realized to be important for protein functions, e.g., in activity-stability trade-offs, how they play a role during enzyme catalysis has been of debate over decades. By studying Pin1 peptidyl-prolyl isomerase using extensive molecular dynamics simulations, here we discuss how the slow intrinsic dynamics of Pin1 observed in the NMR relaxation dispersion experiment occur and couple to isomerization reactions in molecular detail. In particular, we analyze the angular correlation functions of the backbone N–H bonds, and find that slow conformational transitions occur at about the 3_{10} helix in the apo state. These

events at the helical region further affect the residues at about the ligand binding site. Unfolding of this helix leads to a tight hydrogen bond between the helical region and the ligand binding loop, thus forms a stable coiled structure. The helical and coiled structures are found to be characteristic of the Pin1-ligand complex with ligand in the trans and cis states, respectively. These results indicate that the changes in the slow dynamics of Pin1 by isomerization reaction occurs via the shift in populations of the helical and coiled states, where the balance is dependent on the ligand isomerization states.

I. Introduction

Biomolecules constantly fluctuate in solution and often populate a variety of different states.[1–3] Such dynamic nature of proteins are essential for function, and a trade-off between activity and structural stability have been realized.[4–6] Enzyme undergoes different stages during a catalytic cycle such as ligand binding, catalytic reaction, and product release. Multiple intermediates with different chemical states have also been suggested to be important for catalysis.[7,8] Moreover, since the structure as well as chemical state of the ligand change during the reaction cycle, it is expected that enzyme adjusts its structure in order to bind these ligand conformations effectively. The dynamics of enzymes during catalytic cycles have thus been studied extensively using various experimental techniques, e.g. single-molecule Förster resonance energy transfer[9,10] and nuclear magnetic resonance (NMR) relaxation dispersion measurements.[2,11] These studies have highlighted that enzymes show dynamics on the microsecond to millisecond timescale during catalytic cycles, which is comparable to the rate of enzymatic reactions. Yet, how these slow enzyme dynamics play a role in catalytic reactions have been of debate over decades but remains elusive.[12–22]

Peptidyl-prolyl isomerases (PPIases) have been a target to study the dynamics of enzymes during catalysis from both experimental and theoretical perspectives.[22–27] Pin1 is also a member of the PPIase, and selectively catalyzes the isomerization of peptidyl-prolyl bond

between the phosphorylated Ser/Thr (pSer/pThr) and Pro. Pin1 thus connects protein phosphorylation to structural changes, and plays a role in facilitating protein folding, cellular signaling,[28] and gene expression.[29] Pin1 consists of catalytic and WW domains; while ligand binding at the WW domain modulates the catalytic activity in an allosteric manner,[30–33] the catalytic domain maintains the isomerization efficiency even when the allosteric domain is truncated.[34] Pin1 has thus been studied from both experimental and theoretical perspectives to reveal the kinetic and thermodynamic mechanisms, e.g., the free energy of isomerization and turnover rate, and the residues participating in stabilizing the transition state.[34–40]

We have recently studied the dynamics of the isomerization reaction in Pin1 using molecular dynamics (MD) simulations,[41,42] and have revealed that the conformation of Pin1 necessary to stabilize the transition state of isomerization emerge transiently as conformational excited state. Several intra-protein as well as protein-ligand interactions, including the folding/unfolding of 3_{10} helix, were found to be important in the excited state. Indeed, an NMR relaxation dispersion experiment[27] has shown that the 3_{10} helix exhibits a micro- to millisecond dynamics. The NMR result also indicated that the residues with slow dynamics are distributed over multiple residues that surround the ligand binding site. The slow dynamics were observed even in the apo state, and the number of residues showing slow dynamics increased when the ligand is present. Yet, how these slow dynamics are maintained and correlate with ligand binding and catalytic reaction have not been resolved.

To this end, here we study the slow dynamics of Pin1 in the presence and absence of the ligand to reveal how the collective slow dynamics emerge and are affected by ligand in molecular detail. To interpret the dynamics found in the NMR experiment, the angular correlation functions of the backbone N–H bonds are studied using multiple 10 microsecond MD simulations. The dynamics of Pin1 are found to involve events over multiple timescales, thus the distribution of these timescales are analyzed from the inverse Laplace transform of the angular correlation functions. The correlation between the residues are further studied to understand how the slow dynamics over multiple residues are correlated and adapt to

ligands in different isomerization states. This ligand-dependence is expected to appear as changes in apparent slow dynamics during catalytic reaction cycles.

II. Theoretical method

System setup

The structure of the Pin1-ligand complex was taken from the previous work.[41] In brief, the initial complex structure is set up from the catalytic domain (residues 51 to 163) of the crystal structure (PDB: 2Q5A),[43] and the inhibitor in the catalytic site was changed to the widely studied ligand analogue Ace-Ala-Ala-pSer-Pro-Phe-Nme (hereafter labeled as residues 164 to 170).[39,40] The Amber ff99SB-ILDN force field,[44] reoptimized dihedral parameters for the peptide ω-bond angle,[45] and phosphorylated serine parameters by Homeyer et al.[46] were used. Other details including equilibration steps are provided in the previous work.[41]

The structure of the Pin1–ligand complex with the ligand in the cis and trans states were extracted from the previous replica exchange umbrella sampling (REUS) result.[41] 20 snapshots were randomly picked from the REUS trajectories with the isomerization coordinate ζ restrained at 0 and 180 °, which were used for the cis and trans states, respectively. From each snapshot, unbiased MD simulation was performed for 10 μs.

The apo structure was also setup following similar steps as above but without the ligand. After equilibration as described in the previous work,[41] 20 snapshots were prepared by running an unbiased MD simulation for 20 ns and saving the coordinates every 1 ns. From each snapshot, the velocity was re-assigned from a Maxwell-Boltzmann distribution, and MD simulation was performed for 10 μs. All calculations were performed using Amber 20 software package.[47,48]

After MD simulations were performed, each trajectory was aligned against the crystal structure by minimizing the root-mean-square-deviation of the Pin1 backbone heavy atoms between each snapshot and the crystal structure (2Q5A).

Generalized order parameter and relaxation time distribution

Generalized order parameter (S^2) and relaxation time (τ) for the backbone N–H bonds are calculated using the angular correlation function, $C_I(t)$. $C_I(t)$ is defined as[49,50]

$$C_I(t) = \langle P_2\left(\hat{\mu}(t_0) \cdot \hat{\mu}\left(t_0 + t\right)\right)\rangle \tag{1}$$

where $\langle \cdots \rangle$ denotes the time average, $\hat{\mu}$ is a unit vector pointing along the N–H bond, and $P_2(x) = (3x^2/2 - 1/2)$ is the second-order Legendre polynomial. The square of the generalized order parameter, S^2, is given as the long-time limit of $C_I(t)$, i.e.

$$S^2 = \lim_{t\to\infty} C_I(t) \tag{2}$$

Alternatively, S^2 can be also calculated from an equilibrium average over the trajectories as

$$S^2 = \frac{3}{2}\left\{\left\langle x^2\right\rangle^2 + \left\langle y^2\right\rangle^2 + \left\langle z^2\right\rangle^2 + 2\left\langle xy\right\rangle^2 + 2\left\langle yz\right\rangle^2 + 2\left\langle xz\right\rangle^2\right\} - \frac{1}{2} \tag{3}$$

x, y, and z are the projections of $\hat{\mu}$ on the x, y, and z axes. Eqs. (2) and (3) become identical when the trajectory is sufficiently long for the correlation function to have converged. By subtracting the average value S^2, the normalized time correlation function (TCF), $C_0(t)$, is defined as

$$C_0(t) \equiv \frac{C_I(t) - S^2}{1 - S^2} \tag{4}$$

If we naively assume that $C_0(t)$ decays in a single-exponential manner, the relaxation time, τ, can be obtained by integrating $C_0(t)$ over time.[49] In practice, however, $C_0(t)$ decays in a non-exponential manner in most residues (see below). We thus describe the relaxation time with a distribution function of τ, $F(\tau)$, which is obtained by the inverse Laplace transform (iLT) of $C_0(t)$. In practice, we obtain $F(\tau)$ by minimizing the difference between the

data $C_0(t)$ and the mapping of $F(\tau)$ to the t-space using the least-square-fitting

$$\chi^2 = \sum_j^{N_t} \left| C_0(t_j) - \widetilde{C}(t_j) \right|^2 \tag{5}$$

where $\widehat{C}(t)$ is the Laplace transform of $F(\tau)$ given by

$$\widehat{C}(t) = \sum_i^{N_\tau} F(\tau_i) \exp\left(-t/\tau_i\right) \tag{6}$$

Here, N_t and N_τ are the number of grids in the t- and τ-spaces, respectively, where $C_0(t)$ and $F(\tau)$ are discretized. Since this iLT is an ill-conditioned problem, we use the Tikhonov regularization approach, which is also known as L_2-norm or ridge regression.[51,52] The objective function to be minimized is thus

$$Q = \chi^2 - \lambda^2 \Lambda \tag{7}$$

with λ corresponding to the regularization parameter and Λ defined as

$$\Lambda = \sum_{i=1}^{N_\tau} \left| F\left(\tau_i\right) \right|^2 \tag{8}$$

Additionally, we enforce $F(\tau) \geq 0$ considering that relaxation should be described as a sum of positive exponential functions.[53] λ is typically tuned so as to balance χ^2 and Λ. Here, we first calculated the optimal λ for each $F(\tau)$ using the L-curve approach,[54] and subsequently fixed λ to the median of the optimal values ($\lambda = 0.0457$) (Figure S1) in order to use the same value throughout the iLTs for different residues. Note that the choice of λ somewhat alters the height and width of the peaks but do not affect the peak positions.[53] The grids in $t-$ and $\tau-$spaces are taken evenly in log-scale. iLT is performed using $C_0(t)$ for $1 \leq t \leq 2\mu$s since the minimum time step used in calculating $C_0(t)$ is 1 ns and here we are mainly interested in the slowly decaying components.

Generalized correlation from mutual information

In order to quantify the dynamic correlation between residues, the generalized correlation coefficient based on mutual information is calculated.[55] The correlation coefficient between residues i and j is defined as

$$r_{\mathrm{MI}}\left[\mathbf{x}_i, \mathbf{x}_j\right] = \left\{1 - \exp\left(-\frac{2}{3} I\left[\mathbf{x}_i, \mathbf{x}_j\right]\right)\right\}^{1/2} \tag{9}$$

Here, $\mathbf{x}_i$ is the coordinate for residue i and $I\left[\mathbf{x}_i, \mathbf{x}_j\right]$ is the mutual information given by

$$I\left[\mathbf{x}_i, \mathbf{x}_j\right] = \int\int p\left(\mathbf{x}_i, \mathbf{x}_j\right) \ln \frac{p\left(\mathbf{x}_i, \mathbf{x}_j\right)}{p\left(\mathbf{x}_i\right) p\left(\mathbf{x}_j\right)} d\mathbf{x}_i d\mathbf{x}_j \tag{10}$$

where $p(\mathbf{x}_i)$ and $p(\mathbf{x}_i, \mathbf{x}_j)$ are the marginal and joint probability distributions, respectively. For the coordinate $\mathbf{x}_i$, here we use the unit vector along the backbone N–H bond utilized in $C_0(t)$. Since the vector norm is constant, the vector can described by two polar coordinates (θ_i and ψ_i). The marginal and joint probability distributions are thus given in two and four dimensional distribution functions, respectively. While the integral in Eq. (10) needs to be calculated carefully when data points are limited, here we simply evaluate it by summing over the histograms of $p\left(\mathbf{x}_i\right)$ and $p\left(\mathbf{x}_i, \mathbf{x}_j\right)$, considering that the trajectories are sufficiently long. The sensitivity of the results to grid sizes are carefully checked by testing different grid sizes (Fig. S2). The result shows that the grid size of $\leq \pi/10$ is sufficient to identify the correlation while reducing the noise. We thus fix the grid size to be $\pi/10$ in the following analysis.

Correlated motion from time correlation matrix

The slow correlated motion of the protein can also be extracted by analyzing the time correlation matrix. For instance, time-structure based independent component analysis (tICA)[56,57]

solves the generalized eigenvalue problem

$$\mathbf{D}_\tau \mathbf{U}_\tau^{\mathrm{IC}} = \mathbf{D}_0 \mathbf{U}_\tau^{\mathrm{IC}} \mathbf{K}_\tau^{\mathrm{IC}} \tag{11}$$

where τ is the lag time, $\mathbf{U}_\tau^{\mathrm{IC}}$ and $\mathbf{K}_\tau^{\mathrm{IC}}$ are eigenvector and eigenvalue matrices, and $\mathbf{D}_t$ and $\mathbf{D}_0$ are the time correlation and covariance matrices defined by

$$\mathbf{D}_\tau = \left\langle \Delta\mathbf{R}(t_0) \Delta\mathbf{R}(t_0+\tau)^T \right\rangle \tag{12}$$

$$\mathbf{D}_0 = \left\langle \Delta\mathbf{R}(t_0) \Delta\mathbf{R}(t_0)^T \right\rangle \tag{13}$$

Here $\Delta\mathbf{R}(t) = \mathbf{R}(t) - \langle\mathbf{R}\rangle$ and $\mathbf{R}(t)$ is the coordinate set from the trajectory. The independent component (IC) modes are obtained by

$$\mathbf{q}^{\mathrm{IC}}(t)^T = \Delta\mathbf{R}(t)^T \mathbf{U}_\tau^{\mathrm{IC}} \tag{14}$$

Here, we use an alternative approach, dynamic component analysis (DCA),[58] which calculates the slow modes in a two-step manner. DCA solves the eigenvalue problem

$$\widetilde{\mathbf{D}}_\tau \widetilde{\mathbf{U}}_\tau = \widetilde{\mathbf{U}}_\tau \widetilde{\mathbf{\Lambda}}_\tau \tag{15}$$

where $\widetilde{\mathbf{D}}$ is the time correlation matrix

$$\widetilde{\mathbf{D}}_\tau = \left\langle \widetilde{\mathbf{v}}(t_0) \widetilde{\mathbf{v}}(t_0+\tau)^T \right\rangle \tag{16}$$

and $\widetilde{\mathbf{v}}(t)$ is the normalized vector that satisfies $\widetilde{\mathbf{D}}_0 = \left\langle \widetilde{\mathbf{v}}(t_0) \widetilde{\mathbf{v}}(t_0)^T \right\rangle = \mathbf{I}$. Here $\widetilde{\mathbf{D}}_\tau$ is symmetrized ($\widetilde{\mathbf{D}}_{ij} \equiv \frac{1}{2}\left(\widetilde{\mathbf{D}}_\tau^{(ij)} + \widetilde{\mathbf{D}}_\tau^{(ji)}\right)$) to compensate for the limited data and satisfy time-reversibility. $\widetilde{\mathbf{v}}(t)$ is obtained by normalizing the principal component (PC) modes by

$$\widetilde{\mathbf{v}}(t)^T = \Delta\mathbf{R}(t)^T \mathbf{U}_0 \mathbf{K}_0^{-1/2} \tag{17}$$

where $\mathbf{U}_0$ and $\mathbf{K}_0$ are the eigenvector and eigenvalue matrices for the principal component analysis, thus satisfies $\mathbf{D}_0\mathbf{U}_0 = \mathbf{U}_0\mathbf{K}$. The dynamic component (DC) modes are given by

$$\begin{aligned} \mathbf{q}^{\mathrm{DC}}(t)^T &= \Delta\mathbf{R}(t)^T\mathbf{U}_\tau^{\mathrm{DC}} \\ &= \Delta\mathbf{R}(t)^T\mathbf{U}_0\mathbf{K}_0^{-1/2}\widetilde{\mathbf{U}}_\tau \end{aligned} \tag{18}$$

The eigenvalues are sorted in descent order, i.e., the first eigenvector describes the mode with the slowest relaxation time. While the choice of coordinate set $\mathbf{R}$ is arbitrary, here we use the (ϕ, ψ) angles of the backbone to characterize the changes in secondary structure while removing the overall rotational and translational motions. To account for the periodicity of these angles, the cosine and sine of these angles are used as input, thus $\mathbf{R}(t) = (\cos(\psi_{51}), \cos(\phi_{52}), \cos(\psi_{52}), \cdots, \cos(\psi_{163}), \sin(\psi_{51}), \cdots, \sin(\psi_{163}))$ with subscripts being the residue IDs. In order to focus on the slow motions in the microsecond timescale, the lag time τ in constructing $\widetilde{\mathbf{D}}_\tau$ is set to $\tau = 1$ μs, and the subscript τ is hereafter omitted.

Here we note that $\mathbf{q}^{\mathrm{DC}}(t)$ is equivalent to $\mathbf{q}^{\mathrm{IC}}(t)$ when all PC modes are used in constructing $\widetilde{\mathbf{v}}(t)$. However, as seen from Eq. (18), PC modes are divided by the square-root of the PC eigenvalues, i.e., standard deviations of the PC mode trajectories. This means that modes with small fluctuations are amplified, thus DCA using all PC modes as well as tICA suffers from noise by construction. In other words, while elements for these small-amplitude PC modes in the rotation matrix $\widetilde{\mathbf{U}}_\tau$ are often small, the contributions of these modes to $\mathbf{U}_\tau^{\mathrm{DC}}$ ($= \mathbf{U}_\tau^{\mathrm{IC}}$) become large and affects the character of DC as well as IC modes. To overcome this issue, here we restrict the number of PC modes to be used in constructing $\widetilde{\mathbf{D}}_\tau$ in the DCA framework. Hereafter we denote the DC modes constructed using N PC modes as $\mathbf{q}^{\mathrm{DC}(N)}$, e.g. $\mathbf{q}^{\mathrm{DC}(448)} = \mathbf{q}^{\mathrm{IC}}$. This is expected to reduce the noise from $\mathbf{U}^{\mathrm{DC(N)}}$ when characterizing the modes while preserving the slow dynamics.

III. Results and discussion

Slow exchange dynamics from angular correlation

First, the slow relaxations of residues in Pin1 are analyzed using the angular correlation $C_0(t)$ of Pin1's backbone N–H bonds. The results for all residues are given in Figure S3(a), and the values at $t = 1$ μs are plotted in Figure 1 to highlight the residues showing slow decay. The residues with $C_0(t = 1\mu\text{s}) > 0.05$ are further labeled and mapped on the protein structure in Figure 1. The result shows that the residues with notably slow decay are localized at Cys113 to Gly120, which involves the 3_{10} helix. In the apo state, Lys63 to Ile78 and Asp153 to Ser154, which are part of the "ligand binding" and "short" loops, respectively, as well as Lys97, Ser98, and Phe103, located at the C- and N-terminals of two α helices, also decay slowly. Figure 1 also shows that when the ligand binds to Pin1, $C_0(t = 1\mu\text{s})$ becomes smaller in most residues, indicating that ligand binding either reduces the amount of slow component or suppresses slow dynamics. One exception is at about the 3_{10} helix in the trans state showing the increase in $C_0(t)$ especially at Ser114 to Lys117.

To quantify the timescale of slow dynamics from $C_0(t)$, the relaxation time distributions $F(\tau)$ are calculated using iLT. $F(\tau)$ for all residues are summarized in Figure S3(b), and individual curves for the residues with slow relaxations (as labeled in Figure 1) are plotted in Figure 2. We find that in the apo state, most residues plotted in Figure 2 shows a peak at the microsecond time regime. These microsecond components are also found in the ligand bound states, but the amplitudes and peak positions are shifted towards reducing the amount of slow dynamics. Note, however, that in Ser114 to Lys117, the dynamics become somewhat slower when the ligand in the trans state is bound to Pin1.

To further examine how ligand binding affects the slow dynamics of Pin1, the slowest relaxation time for each residue, estimated from the peak position of $F(\tau)$ given in Figure S3(b), is summarized in Figure 3. Here we omit the shallow peaks (i.e. peak maximum lower than 0.1) which may have appeared due to lack of sufficient sampling. The result shows that

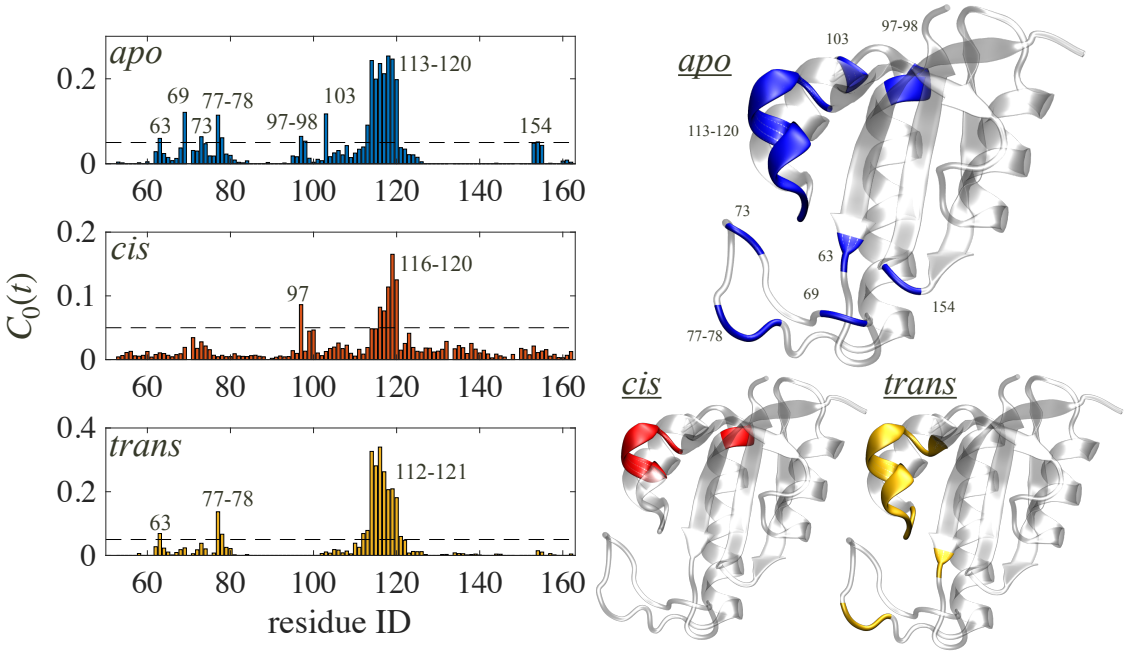

Figure 1: Angular correlation function $C_0(t)$ at 1 μs ($C_0(t = 1\mu s)$)for the apo (top), cis (middle), and trans (bottom) states. Labels denote the residues with $C_0(t = 1\mu s) > 0.05$, and these residues are colored in the structures of Pin1 (with coordinates from PDB: 2Q5A) on right.

residues exhibiting microsecond relaxation time is reduced from 15 to 7 and 11 in the apo to cis and trans states, respectively. Microsecond dynamics are present only at residues 97, 99, and 100, and 116 to 120 in the cis state, whereas they appear in 63, 77, 112 to 120 in the trans state. On the other hand, many residues in the cis state exhibit a peak at ∼600 ns, which implies that collective dynamics at this timescale are present. These results thus indicate that while slow dynamics are present in all three states, the dynamics are reduced at most residues when the ligand is bound. Here we note that, in the NMR experiment,[27] Arg69 and Cys113 to Ser115 (Group A) and Gln75 to Lys77 (Group B) were found to show slow exchange dynamics with a rate of 1200 s^{-1} and 5000 s^{-1}, respectively, in the apo state. Although the timescales estimated in the experiment are too slow compared to what MD simulations can access, the residues involved in these slow dynamics are in notable agreement with the MD result. On the other hand, the same work also indicated that when the ligand is present, the number of residues involved in Group A are increased, which involves Arg68,

Arg69, Ser154, and Gly155; the rates changed to 1500 s^{-1} and 3500 s^{-1} for Groups A and B, respectively. This is in contrast to the current result, yet it is important to note that the slow dynamics in the NMR experiment[27] also involves isomerization events. Thus ligand isomerizations can also contribute to slow dynamics by shifting the equilibrium structure if they differ before and after the reaction.

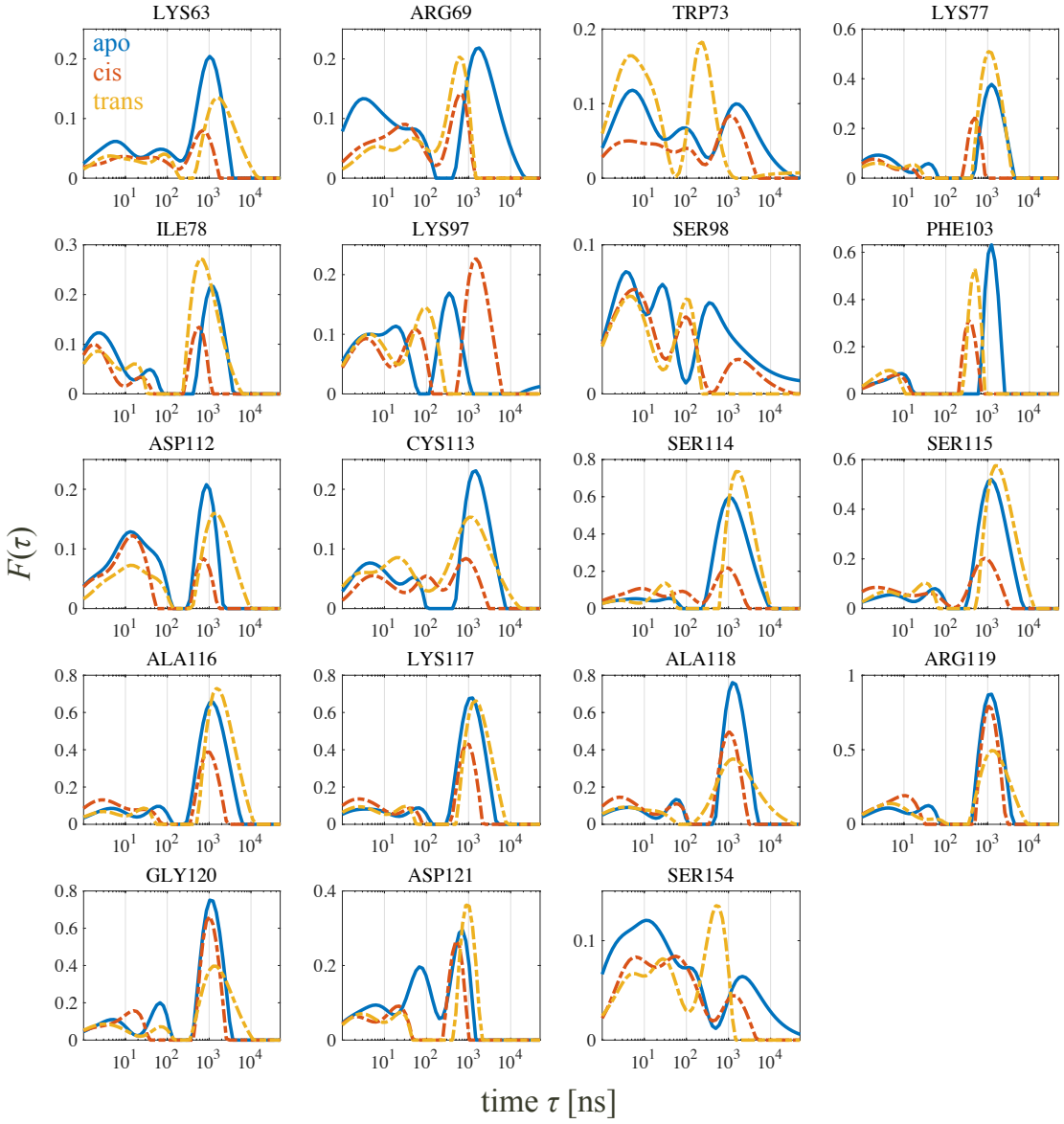

Figure 2: Relaxation time distribution functions $F(\tau)$ for the residues with slow relaxation of $C_0(t)$ labeled in Figure 1. Blue, red, and yellow lines are the results for the apo, cis, and trans states, respectively.

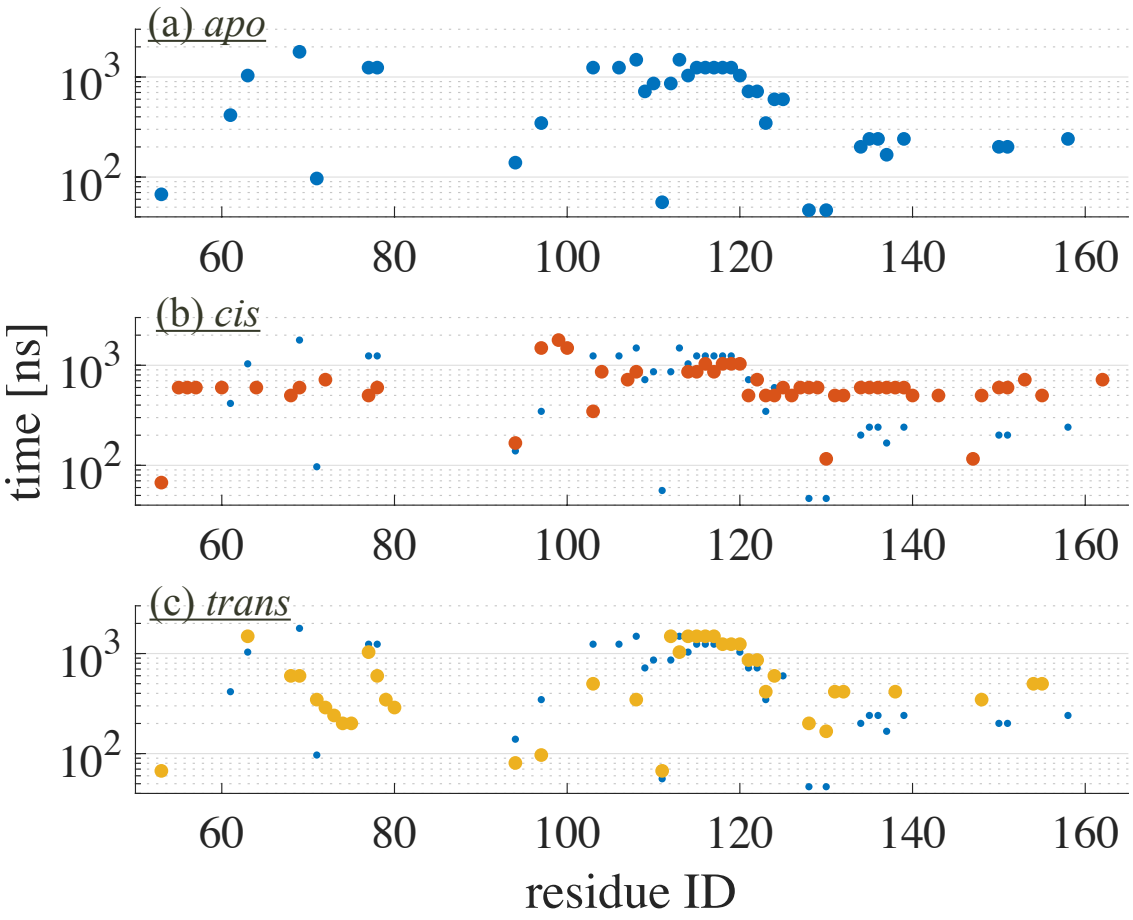

Figure 3: Slowest relaxation time of each residue determined from the peak of $F(\tau)$ for (a) apo, (b) cis, and (c) trans states. Only the peaks higher than 0.1 are considered. The blue points in (b) and (c) show the result of (a) (apo state) to highlight the changes triggered by ligand binding.

Changes in structure from order parameter

We next compare the order parameter S^2, calculated using Eq. 3, to examine how the structures and conformational flexibilities differ among the apo, cis, and trans states. The raw S^2 values for all residues and the differences (ΔS^2) between the apo, cis, and trans states are given in Figures S4 and 4, respectively. Figure 4 shows that, upon ligand bind, S^2 increases most prominently at residues 114 to 120. The residues in the ligand binding (Lys63 to Arg80) and short (Ser154 to Ile156) loops also show positive ΔS^2. This change in S^2 is consistent with previous studies showing that Arg68, Arg69, Cys113, and Ser154 strongly interacts with the ligand in the ligand-Pin1 complex.[39–41,59,60] We also see that increase in S^2 is more pronounced in the cis state compared to that in the trans state, especially at the C-terminal half of the ligand binding loop (e.g. Trp73 to Ile78) and the residues at about the N-terminal of 3_{10} helix (Ser111 to Ser115) (Fig. 4(c)). This indicates that conformational flexibility is reduced in the cis state than in trans state. Comparison of Figures 4 and 1 highlights that the residues with a notable increase in ΔS^2 match remarkably well with those showing slow relaxation of $C_0(t)$ in the apo state. These results show that the residues participating in ligand binding highly overlap with those exhibiting slow dynamics, and indicates that slow dynamics of Pin1 are reduced by ligand binding.

Molecular origin of slow conformational dynamics

While ΔS^2 in Figure 4 shows that residues 113 to 120 become rigid when the ligand is bound in the cis and trans states, our previous result[41] has indicated that the 3_{10} helix is formed only in the trans state. To reveal the molecular origin of this seeming discrepancy, hydrogen bond patterns at about the 3_{10} helix are analyzed. In particular, a hydrogen bond between Cys113(O) and Ala116(H) is found frequently when the 3_{10} helix is present. The distributions of the Cys113(O)-Ala116(H) distance, given in Figure 5(a), indeed show that a sharp peak at < 3.0 Å is present in the trans state. A small peak is also seen in the apo state, but disappears in the cis state. Instead, Figure 5(b) shows that a strong hydrogen bond between

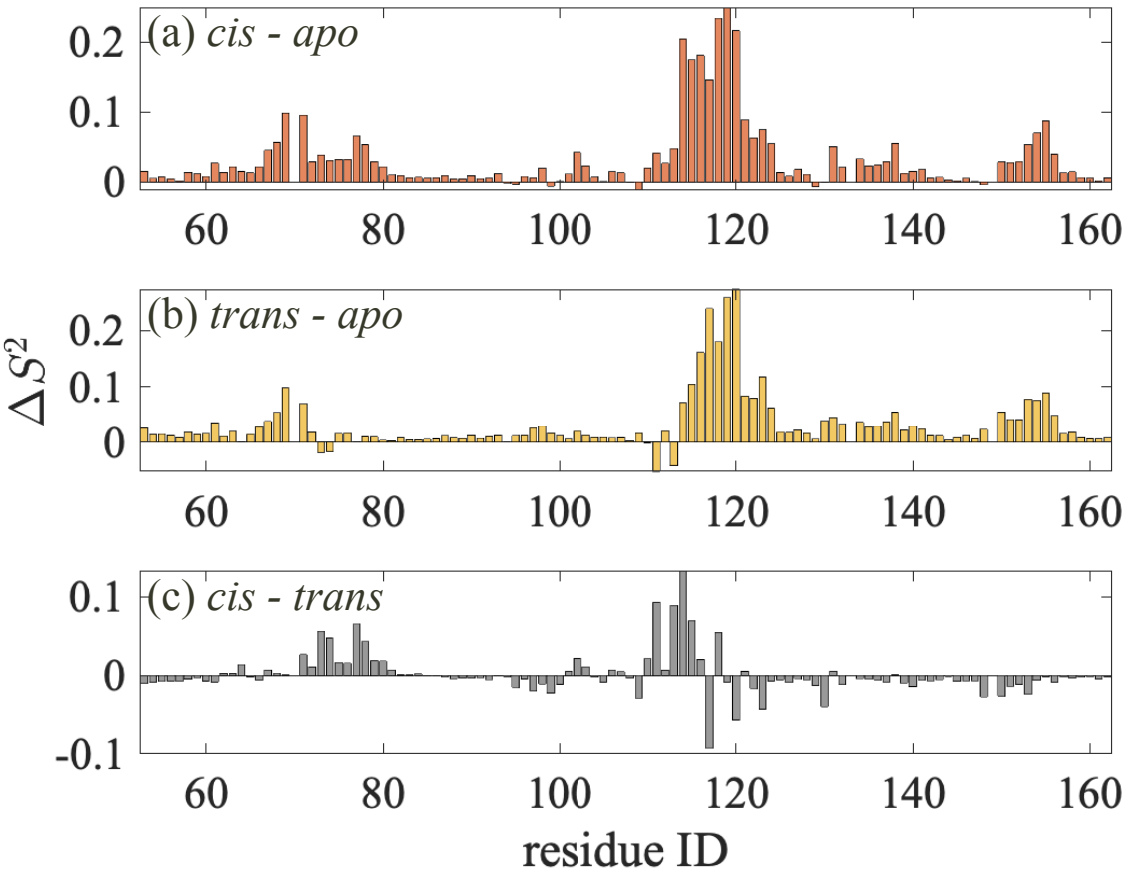

Figure 4: Differences in the order parameter (ΔS^2) for the backbone N–H bonds between (a) cis and apo, (b) trans and apo, and (c) cis and trans states. The raw S^2 data are given in Figure S4.

Cys113(O) and Thr73(H) is found in the cis state. This hydrogen bond is almost fully conserved in the cis state, thus can be regarded as a characteristic "coiled" structure when the 3_{10} helix is unfolded (Figure 5(c)). Moreover, the hydrogen bond between Cys113(O) and Thr73(H) is found in the apo as well as trans states, indicating that conformational transitions between the 3_{10} helix and coiled states are intrinsic in Pin1, and the balance between the two states are determined by the presence of ligand as well as its isomerization state. The TCF of the Cys113(O)-Ala116(H) distance and its relaxation time distribution, given in Figure 6, show that the transitions between the two states occur in the microsecond timescale. The rate becomes slightly slower in the trans state compared to that in the apo state, which may be due to the 3_{10} helix being more stable when the ligand in the trans state is bound.

We note that Cys113(O)-Thr73(H) hydrogen bond not only locks Thr73, but further affects the dynamics of the ligand binding loop (residues 69 to 78). To analyze the correlation of motions between these residues in more detail, the generalized correlation coefficient based on mutual information of the N–H vectors is analyzed. The coefficient matrix $\mathbf{r}_{\mathrm{MI}}$ for the apo state is given in Figure 7, whereas those for the cis and trans states are summarized in Figure S5. Figure 7 shows that $\mathbf{r}_{\mathrm{MI}}$ about the 3_{10} helix (residues 113 to 120) is large, indicating that helix folding/unfolding is a highly correlated event. The correlation within the ligand binding loop is also strong, and the motions at this loop are correlated with the 3_{10} helix regime through residues Trp73 and Arg74, as seen in the off-diagonal elements in Figure 7. Similarly, we find correlations in motions between the N-terminal of the ligand binding loop (residue 68 and 69) and the short loop (residues 153 and 155). This correlation is maintained through the hydrogen bond between Arg68(H) and Asp153(O). Thus, the slow conformational change at about the 3_{10} helix (residues 113 to 120) is "communicated" to the ligand binding loop (residues 71 to 80), and is further transmitted to the short loop (residues 153 to 155), resulting in correlated slow dynamics at different regions of the protein that surround the ligand binding pocket. Moreover, the difference in S^2 between the cis and

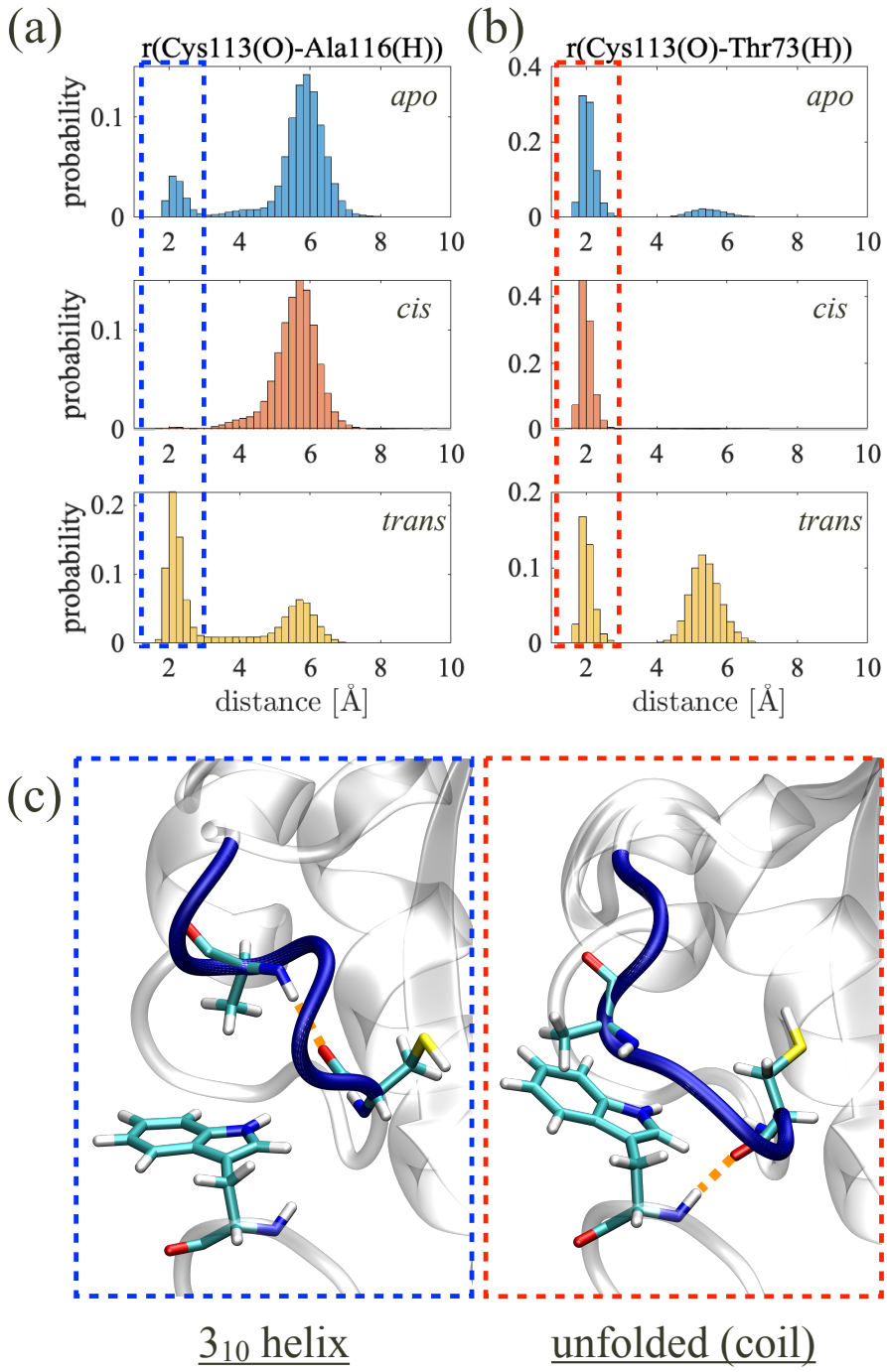

Figure 5: Histograms of the distances between (a) Cys113(O) and Ala116(H) and (b) Cys113(O) and Thr73(H). Blue (top), red (center), and yellow (bottom) histograms show the results for the apo, cis, and trans states, respectively. The boxes in dashed lines highlight the peaks with the distances below 3Å. (c) Characteristic structures where the Cys113(O)-Ala116(H) (left) and Cys113(O)-Thr73(H) (right) distances (orange dashed lines) are ∼2 Å.

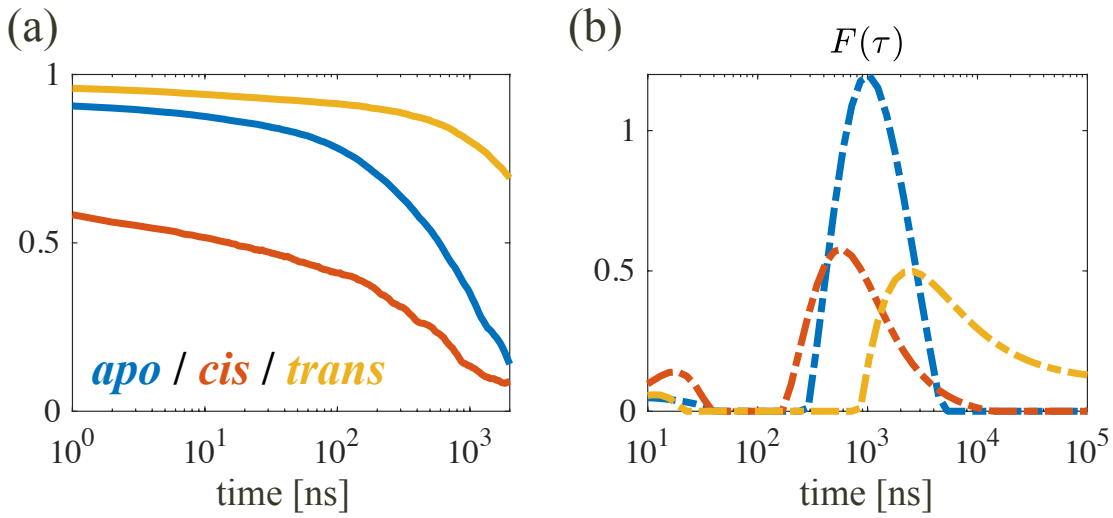

Figure 6: (a) Time correlation functions of the distance between Cys113(O) and Ala116(H), and (b) their relaxation time distributions calculated using iLT. Blue, red, and yellow lines denote the results for the apo, cis, and trans states, respectively.

trans states (Figure 4) as well as their structural analyses (Fig. 5) indicate that the mean structure differs between the cis and trans states. This will result in an apparent slow dynamics coupled to isomerization reaction events, even though the dynamics within the cis and trans states are suppressed as shown above (Fig. 2). Overall, these dynamic events are expected to appear as slow dynamics in the Pin1-ligand complex in the NMR experiment.[27]

Characterization of the slowest correlated motion

Finally we examine the trajectory of Pin1 in the apo state to investigate collective motions with slow dynamics using the DCA method. As seen from Fig. S6, the TCFs calculated from the trajectories of DC1 and DC2 are found to relax notably slower than the other modes. The trajectories of DC1 and DC2, given in Fig. S7(a), shows that DC1 captures a very rare event that occurred only once throughout the 20 trajectories, whereas DC2 describes the transitions that occur infrequently but in multiple trajectories. When the trajectories constructed using different number of PCs as in Eq. (16) are compared, we find that 50 and even 20 PC modes seems sufficient to capture the character. The TCFs and their relaxation

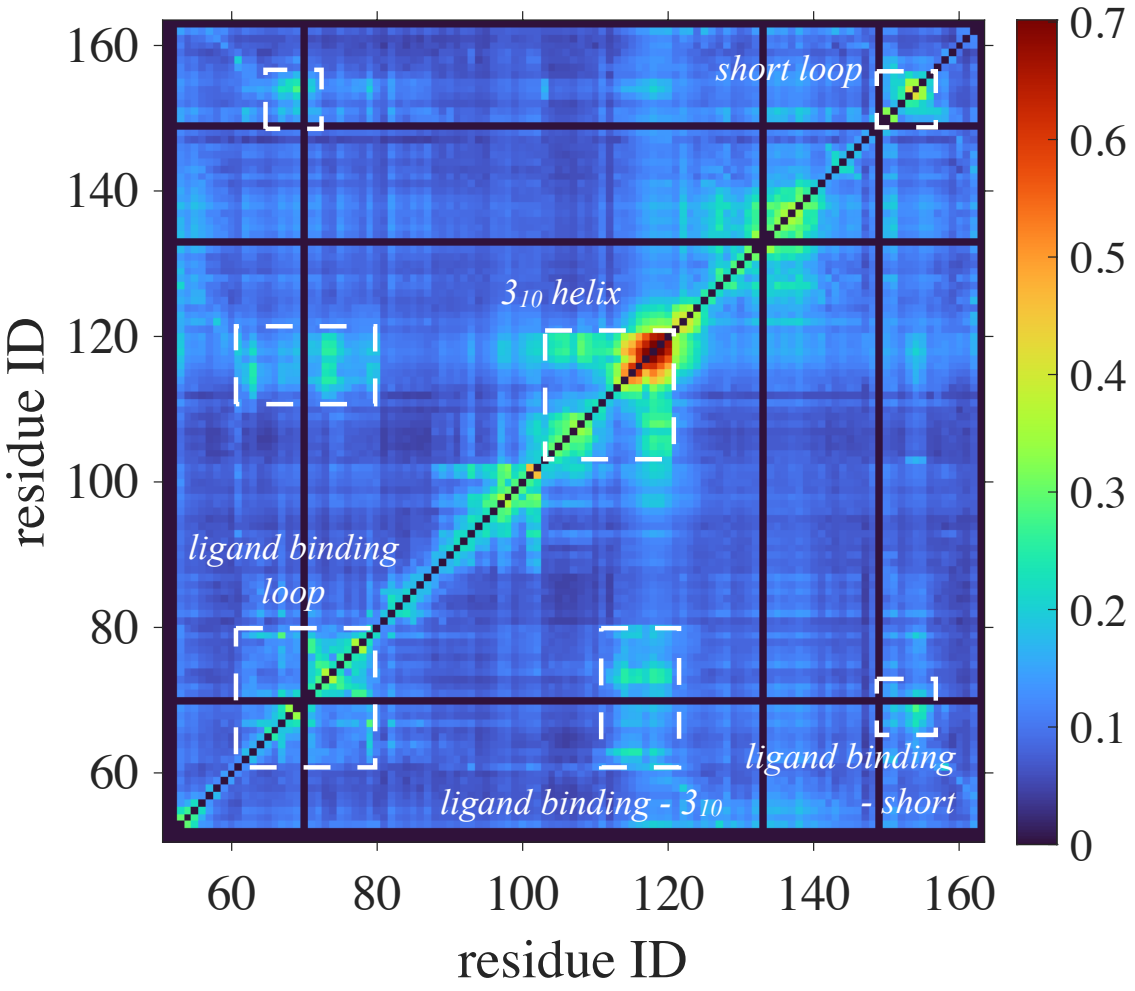

Figure 7: Generalized correlation coefficients based on mutual information for the apo state. Residual interactions are calculated using the backbone N–H bonds. Diagonal terms are also set to zero. The ligand binding loop, 3_{10} helix, and short loop as well as their correlations are highlighted in white boxes. The results for the ligand bound states are provided in Figure S5.

time distributions, given in Figs. S8 and S9, indeed reveals that $\mathbf{q}^{\mathrm{DC}(20)}$ sufficiently capture the essential slow dynamics found in the $\mathbf{q}^{\mathrm{IC}}$. Here we note that the timescale for the relaxation of DC1 cannot be estimated properly since only one transition is found in the trajectories.

We next analyze the coordinates contributing to DC modes. Figs. 8 and 9 show the conversion matrix $\mathbf{U}^{\mathrm{DC}}$ (Eq. 18) for DC1 and DC2, respectively. We see that DC1 largely consists of changes in residues 102, 103, and 152 to 155. Comparison of Figs. 8(a) and 8(b) indicates that while the essential components are similar, DC(448) appears to involve many non-zero components. This character becomes more evident in DC2, i.e. DC(448) cannot distinguish the important components from the "noise". In contrast, DC(20) finds that DC2 mainly consists of changes in the ligand binding loop (residues 68, 69, 76, and 77), 3_{10} helix (117, 119, and 120), and short loop (153 to 155). These results show that despite the differences in timescales studied in the simulation and experiment, DC1 and DC2 extracts the coupled motions of residues exhibiting slow dynamics as Group A and B in the experiment. The rate estimated from the DC modes are slightly slower than those from the angular relaxation of individual N–H vectors, likely due to coupling between motions. DCA thus indicates that slow collective motions between residues about the catalytic pocket exist, which confirms the correlation found in $\mathbf{r}_{\mathrm{MI}}$ (Fig. 7).

IV. Summary

NMR relaxation dispersion measurements have shown that Pin1 involves micro- to millisecond dynamics in the apo state,[27] and that the dynamics correlate with the timescale of isomerization reaction. This implies that the slow dynamics of Pin1 is necessary for the reaction and the slow dynamics are intrinsically embedded in Pin1 even when the ligand is absent.

In order to elucidate the molecular mechanism behind the changes in Pin1's slow dy-

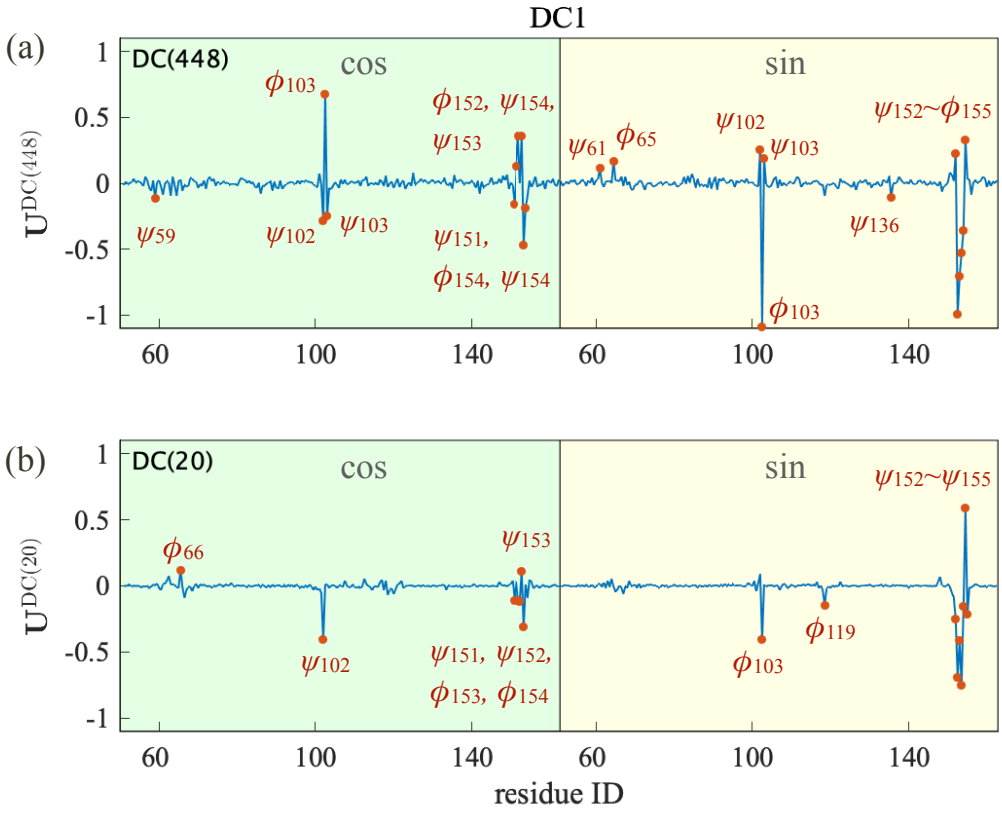

Figure 8: Coordinates contributing to DC1 in (a) $\mathbf{U}^{\mathrm{DC(448)}}$ and (b) $\mathbf{U}^{\mathrm{DC(20)}}$. Green and yellow regions describe the torsion angles in cosine and sine forms. The components with the absolute value larger than 0.1 are marked in red points with labels.

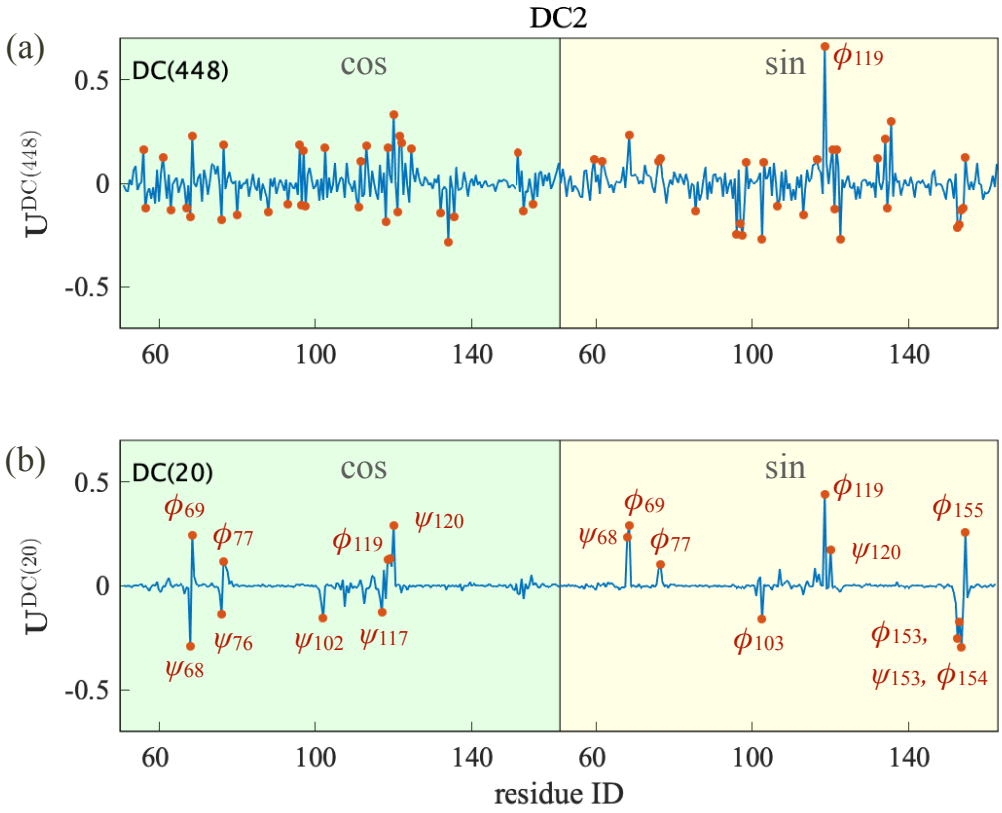

Figure 9: Coordinates contributing to DC2 in (a) $\mathbf{U}^{\mathrm{DC(448)}}$ and (b) $\mathbf{U}^{\mathrm{DC(20)}}$. Green and yellow regions describe the torsion angles in cosine and sine forms. The components with the absolute value larger than 0.1 are marked in red points with labels.

namics, here we studied the dynamics of Pin1 in the apo as well as ligand bound states using multiple 10 μs MD simulations. The angular correlation functions of the backbone N–H bonds showed that slow dynamics are found most prominently at about the 3_{10} helix. The slow dynamics were also found at the ligand binding as well as short loops, which interact with the ligand when the ligand is bound. The timescales of these slow dynamics were estimated to be on microseconds from the relaxation time distributions obtained by inverse Laplace transform of the angular correlation functions. The result for the ligand bound complex, on the other hand, showed that slow dynamics are reduced when the ligand is bound. This trend appears to contradict the NMR experiment.[27]

To understand the origin of this seeming discrepancy, the structural rigidness of Pin1 was analyzed using the order parameter S^2. The result showed that S^2 is increased upon ligand binding, which is in line with the decrease of slow dynamics in the ligand bound state. The difference of S^2 between the cis- and trans-ligand bound complexes, on the other hand, indicates that major structures in the two states are different. By analyzing the structure ensembles of the ligand-bound complexes in more detail, we found that the 3_{10} helix is formed in the trans state, whereas the helix is unfolded in the cis state. Instead, a characteristic coiled structure with a strong hydrogen bond between Cys113(O) and Thr73(H) was found in the cis state. Furthermore, the transitions between the helical and coiled states were observed in the apo state, with the timescale of the transitions estimated to be on the order of microseconds. Note that the 3_{10} helix was also found to be unstable in previous MD simulations.[32,41]

By analyzing the residual correlations based on the mutual information, the conformational dynamics at about the 3_{10} helix region were found to affect the ligand binding loop via Trp73 and Arg74; the dynamics were further communicated within this loop and to the short loop through a hydrogen bond between Arg68(H) and Asp153(O). Thus, the slow dynamics at different residues found in the apo state were connected by a network of residues mediated by the ligand binding loop. The analysis of time correlation matrix via DCA further

confirmed that the ligand binding loop, 3_{10} helix, and short loop moves in a collective manner in the microsecond timescale. We also note that DCA constructed from 20 PC modes was able to characterize this collective motion, whereas DCA using all PC modes, which is equivalent to tICA, suffered from noise that originates from small amplitude PC modes. Although the MD simulation performed here is not sufficient to distinguish the slow modes, e.g. those consisting Group A and B in the NMR experiment, the current result indicates that DCA can be applied to characterize the intrinsic slow motions involved in catalysis when sufficiently long MD simulation is performed.

Finally, the difference in equilibrium structures between the cis and trans states are expected to exhibit slow dynamics coupled to isomerization reactions as a result of population shift. Here we emphasize that the slow protein dynamics are not directly coupled to isomerization transitions at the ligand, since the isomerzation events are expected to occur locally and rapidly (at $\sim$ ps) from the conformational excited state.[41] On the other hand, the formation of proper interactions, e.g., 3_{10} helix and the hygrogen bond between the catalytic and short loops, is essential for the excited state and near the transition state. Thus, the slow dynamics of Pin1 do not play a direct role in catalytic reaction events, but are nevertheless important for the catalytic activity by tuning the structure of Pin1 in the bound state in a ligand-specific manner as well as by accessing the excited state. We also note that, when the WW domain is present, dynamic allostery is observed when a ligand is bound to the WW domain. To what extent does this ligand binding affects the slow dynamics observed in the current manuscript is to be studied in future work. Whether the slow intrinsic dynamics of other enzymes including PPIases also play similar roles during catalysis are currently under investigation.

Acknowledgement

This work was supported by Grant-in-Aid for Scientific Research (18K05049 and 22H02035

to T.M. and 21H04676 to S.S.) from JSPS. The calculations are partially carried out at the Research Center for Computational Sciences in Okazaki (21-IMS-C124). T.M. also acknowledges the support from Pan-Omics Data-Driven Research Innovation Center, Kyushu University.

Supporting Information Available

Histogram of the regularization parameter used in iLT, angular correlation, relaxation distribution functions, and order parameters of the backbones for all residues, generalized correlation matrices for ligand bound states, time correlation functions for DC modes, the trajectories along DC modes, and the relaxation time distributions of DC modes. The Supporting Information is available free of charge on the ACS publications website.

References

(1) English, B. P.; Min, W.; Van Oijen, A. M.; Kang, T. L.; Luo, G.; Sun, H.; Cherayil, B. J.; Kou, S. C.; Xie, X. S. Ever-fluctuating single enzyme molecules: Michaelis-Menten equation revisited. *Nat. Chem. Biol.* **2006**, *2*, 87–94.

(2) Boehr, D. D.; Dyson, H. J.; Wright, P. E. An NMR perspective on enzyme dynamics. *Chem. Rev.* **2006**, *106*, 3055–3079.

(3) Henzler-Wildman, K.; Kern, D. Dynamic personalities of proteins. *Nature* **2007**, *450*, 964–972.

(4) Beadle, B. M.; Shoichet, B. K. Structural bases of stability-function tradeoffs in enzymes. *J. Mol. Biol.* **2002**, *321*, 285–296.

(5) Siddiqui, K. S.; Cavicchioli, R. Cold-adapted enzymes. *Annu. Rev. Biochem.* **2006**, *75*, 403–433.

(6) Couñago, R.; Wilson, C. J.; Peña, M. I.; Wittung-Stafshede, P.; Shamoo, Y. An adaptive mutation in adenylate kinase that increases organismal fitness is linked to stabilityactivity trade-offs. *Protein Eng. Des. Sel.* **2008**, *21*, 19–27.

(7) Boehr, D. D.; McElheny, D.; Dyson, H. J.; Wrightt, P. E. The dynamic energy landscape of dihydrofolate reductase catalysis. *Science* **2006**, *313*, 1638–1642.

(8) Hammes, G. G.; Benkovic, S. J.; Hammes-Schiffer, S. Flexibility, diversity, and cooperativity: Pillars of enzyme catalysis. *Biochemistry* **2011**, *50*, 10422–10430.

(9) Roy, R.; Hohng, S.; Ha, T. A practical guide to single-molecule FRET. *Nat. Methods* **2008**, *5*, 507–516.

(10) Yang, H.; Luo, G.; Karnchanaphanurach, P.; Louie, T. M.; Rech, I.; Cova, S.; Xun, L.; Xie, X. S. Protein conformational dynamics probed by single-molecule electron transfer. *Science* **2003**, *302*, 262–266.

(11) Ishima, R.; Torchia, D. A. Protein dynamics from NMR. *Nat. Struct. Biol.* **2000**, *7*, 740–743.

(12) Watt, E. D.; Shimada, H.; Kovrigin, E. L.; Loria, J. P. The mechanism of rate-limiting motions in enzyme function. *Proc. Natl. Acad. Sci. U. S. A.* **2007**, *104*, 11981–11986.

(13) Henzler-Wildman, K. A.; Lei, M.; Thai, V.; Kerns, S. J.; Karplus, M.; Kern, D. A hierarchy of timescales in protein dynamics is linked to enzyme catalysis. *Nature* **2007**, *450*, 913–916.

(14) Pisliakov, A. V.; Kamerlin, S. C. L.; Warshel, A. Enzyme millisecond conformational dynamics do not catalyze the chemical step. *Proc. Natl. Acad. Sci. U. S. A.* **2009**, *106*, 17359–17364.

(15) Schwartz, S. D.; Schramm, V. L. Enzymatic transition states and dynamic motion in barrier crossing. *Nat. Chem. Biol.* **2009**, *5*, 551–558.

(16) Nagel, Z. D.; Klinman, J. P. A 21st century revisionist's view at a turning point in enzymology. *Nat. Chem. Biol.* **2009**, *5*, 543–550.

(17) Luk, L. Y. P.; Loveridge, E. J.; Allemann, R. K. Protein motions and dynamic effects in enzyme catalysis. *Phys. Chem. Chem. Phys.* **2015**, *17*, 30817–30827.

(18) Kamerlin, S. C.; Warshel, A. At the dawn of the 21st century: Is dynamics the missing link for understanding enzyme catalysis. *Proteins* **2010**, *78*, 1339–1375.

(19) Kohen, A. Role of dynamics in enzyme catalysis: Substantial versus semantic controversies. *Acc. Chem. Res.* **2015**, *48*, 466–473.

(20) Hanoian, P.; Liu, C. T.; Hammes-Schiffer, S.; Benkovic, S. Perspectives on electrostatics and conformational motions in enzyme catalysis. *Acc. Chem. Res.* **2015**, *48*, 482–489.

(21) Bhabha, G.; Biel, J. T.; Fraser, J. S. Keep on moving: Discovering and perturbing the conformational dynamics of enzymes. *Acc. Chem. Res.* **2015**, *48*, 423–430.

(22) Eisenmesser, E. Z.; Millet, O.; Labeikovsky, W.; Korzhnev, D. M.; Wolf-Watz, M.; Bosco, D. A.; Skalicky, J. J.; Kay, L. E.; Kern, D. Intrinsic dynamics of an enzyme underlies catalysis. *Nature* **2005**, *438*, 117–121.

(23) Eisenmesser, E. Z.; Bosco, D. A.; Akke, M.; Kern, D. Enzyme dynamics during catalysis. *Science* **2002**, *295*, 1520–1523.

(24) Agarwal, P. K. Role of protein dynamics in reaction rate enhancement by enzymes. *J. Am. Chem. Soc.* **2005**, *127*, 15248–15256.

(25) Doshi, U.; McGowan, L. C.; Ladani, S. T.; Hamelberg, D. Resolving the complex role of enzyme conformational dynamics in catalytic function. *Proc. Natl. Acad. Sci. U. S. A.* **2012**, *109*, 5699–5704.

(26) Wapeesittipan, P.; Mey, A. S.; Walkinshaw, M. D.; Michel, J. Allosteric effects in cyclophilin mutants may be explained by changes in nano-microsecond time scale motions. *Commun. Chem.* **2019**, *2*, 41.

(27) Labeikovsky, W.; Eisenmesser, E. Z.; Bosco, D. A.; Kern, D. Structure and Dynamics of Pin1 During Catalysis by NMR. *J. Mol. Biol.* **2007**, *367*, 1370–1381.

(28) Lu, K. P.; Hanes, S. D.; Hunter, T. A human peptidyl-prolyl isomerase essential for regulation of mitosis. *Nature* **1996**, *380*, 544–547.

(29) Zhang, M.; Wang, X. J.; Chen, X.; Bowman, M. E.; Luo, Y.; Noel, J. P.; Ellington, A. D.; Etzkorn, F. A.; Zhang, Y. Structural and kinetic analysis of prolyl-isomerization/phosphorylation cross-talk in the CTD code. *ACS Chem. Biol.* **2012**, *7*, 1462–1470.

(30) Namanja, A. T.; Wang, X. J.; Xu, B.; Mercedes-Camacho, A. Y.; Wilson, K. A.; Etzkorn, F. A.; Peng, J. W. Stereospecific gating of functional motions in Pin. *Proc. Natl. Acad. Sci. U. S. A.* **2011**, *108*, 12289–12294.

(31) Wilson, K. A.; Bouchard, J. J.; Peng, J. W. Interdomain interactions support interdomain communication in human pin1. *Biochemistry* **2013**, *52*, 6968–6981.

(32) Guo, J.; Pang, X.; Zhou, H. X. Two pathways mediate interdomain allosteric regulation in Pin1. *Structure* **2015**, *23*, 237–247.

(33) Barman, A.; Hamelberg, D. Coupled Dynamics and Entropic Contribution to the Allosteric Mechanism of Pin1. *J. Phys. Chem. B* **2016**, *120*, 8405–8415.

(34) Greenwood, A. I.; Rogals, M. J.; De, S.; Lu, K. P.; Kovrigin, E. L.; Nicholson, L. K. Complete determination of the Pin1 catalytic domain thermodynamic cycle by NMR lineshape analysis. *J. Biomol. NMR* **2011**, *51*, 21–34.

(35) Dugave, C.; Demange, L. Cis-trans isomerization of organic molecules and biomolecules: Implications and applications. *Chem. Rev.* **2003**, *103*, 2475–2532.

(36) Behrsin, C. D.; Bailey, M. L.; Bateman, K. S.; Hamilton, K. S.; Wahl, L. M.; Brandl, C. J.; Shilton, B. H.; Litchfield, D. W. Functionally Important Residues in the Peptidyl-prolyl Isomerase Pin1 Revealed by Unigenic Evolution. *J. Mol. Biol.* **2007**, *365*, 1143–1162.

(37) Xu, N.; Tochio, N.; Wang, J.; Tamari, Y.; Uewaki, J. I.; Utsunomiya-Tate, N.; Igarashi, K.; Shiraki, T.; Kobayashi, N.; Tate, S. I. The C113D mutation in human Pin1 causes allosteric structural changes in the phosphate binding pocket of the ppiase domain through the tug of war in the dual-histidine motif. *Biochemistry* **2014**, *53*, 5568–5578.

(38) Vöhringer-Martinez, E.; Duarte, F.; Toro-Labbé, A. How does pin1 catalyze the cis-trans prolyl peptide bond isomerization? A QM/MM and mean reaction force study. *J. Phys. Chem. B* **2012**, *116*, 12972–12979.

(39) Velazquez, H. A.; Hamelberg, D. Conformation-directed catalysis and coupled enzyme-substrate dynamics in Pin1 phosphorylation-dependent cis-trans isomerase. *J. Phys. Chem. B* **2013**, *117*, 11509–11517.

(40) Di Martino, G. P.; Masetti, M.; Cavalli, A.; Recanatini, M. Mechanistic insights into Pin1 peptidyl-prolyl cis-trans isomerization from umbrella sampling simulations. *Proteins* **2014**, *82*, 2943–2956.

(41) Mori, T.; Saito, S. Conformational Excitation and Nonequilibrium Transition Facilitate Enzymatic Reactions: Application to Pin1 Peptidyl-Prolyl Isomerase. *J. Phys. Chem. Lett.* **2019**, *10*, 474–480.

(42) Mori, T.; Saito, S. Dissecting the Dynamics during Enzyme Catalysis: A Case Study of Pin1 Peptidyl-Prolyl Isomerase. *J. Chem. Theory Comput.* **2020**, *16*, 3396–3407.

(43) Zhang, Y.; Daum, S.; Wildermann, D.; Zhou, X. Z.; Verdecia, M. A.; Bowman, M. E.; Lücke, C.; Hunter, T.; Lu, K. P.; Fischer, G.; Noel, J. P. Structural basis for high-affinity peptide inhibition of human Pin1. *ACS Chem. Biol.* **2007**, *2*, 320–328.

(44) Lindorff-Larsen, K.; Piana, S.; Palmo, K.; Maragakis, P.; Klepeis, J. L.; Dror, R. O.; Shaw, D. E. Improved side-chain torsion potentials for the Amber ff99SB protein force field. *Proteins* **2010**, *78*, 1950–1958.

(45) Doshi, U.; Hamelberg, D. Reoptimization of the AMBER force field parameters for peptide bond (Omega) torsions using accelerated molecular dynamics. *J. Phys. Chem. B* **2009**, *113*, 16590–16595.

(46) Homeyer, N.; Horn, A. H.; Lanig, H.; Sticht, H. AMBER force-field parameters for phosphorylated amino acids in different protonation states: Phosphoserine, phosphothreonine, phosphotyrosine, and phosphohistidine. *J. Mol. Model.* **2006**, *12*, 281–289.

(47) Case, D. A.; Belfon, K.; Ben-Shalom, I. Y.; Brozell, S. R.; Cerutti, D. S.; Cruzeiro, V. W. D.; Darden, T. A.; Duke, R. E.; Giambasu, G.; et al., Amber 20. 2021.

(48) Salomon-Ferrer, R.; Götz, A. W.; Poole, D.; Le Grand, S.; Walker, R. C. Routine microsecond molecular dynamics simulations with AMBER on GPUs. 2. Explicit solvent particle mesh ewald. *J. Chem. Theory Comput.* **2013**, *9*, 3878–3888.

(49) Chatfield, D. C.; Szabo, A.; Brooks, B. R. Molecular dynamics of staphylococcal nuclease: Comparison of simulation with 15N and 13C NMR relaxation data. *J. Am. Chem. Soc.* **1998**, *120*, 5301–5311.

(50) Lipari, G.; Szabo, A. Model-Free Approach to the Interpretation of Nuclear Magnetic Resonance Relaxation in Macromolecules. 1. Theory and Range of Validity. *J. Am. Chem. Soc.* **1982**, *104*, 4546–4559.

(51) Eldén, L. Algorithms for the regularization of ill-conditioned least squares problems. *BIT Numer. Math.* **1977**, *17*, 134–145.

(52) Bishop, C. M. *Springer-Verlag New York, Inc.,, Secaucus, NJ, USA*; Springer, New York, 2006; p 9.

(53) Ono, J.; Takada, S.; Saito, S. Couplings between hierarchical conformational dynamics from multi-time correlation functions and two-dimensional lifetime spectra: Application to adenylate kinase. *J. Chem. Phys.* **2015**, *142*, 212404.

(54) Hansen, P. C.; OLeary, D. P. The Use of the L-Curve in the Regularization of Discrete Ill-Posed Problems. *SIAM J. Sci. Comput.* **1993**, *14*, 1487–1503.

(55) Lange, O. F.; Grubmüller, H. Generalized correlation for biomolecular dynamics. *Proteins* **2006**, *62*, 1053–1061.

(56) Pérez-Hernández, G.; Paul, F.; Giorgino, T.; De Fabritiis, G.; Noé, F. Identification of slow molecular order parameters for Markov model construction. *J. Chem. Phys.* **2013**, *139*, 15102.

(57) Naritomi, Y.; Fuchigami, S. Slow dynamics in protein fluctuations revealed by time-structure based independent component analysis: The case of domain motions. *J. Chem. Phys.* **2011**, *134*, 65101.

(58) Mori, T.; Saito, S. Dynamic heterogeneity in the folding/unfolding transitions of FiP35. *J. Chem. Phys.* **2015**, *142*.

(59) Moritsugu, K.; Yamamoto, N.; Yonezawa, Y.; Tate, S. I.; Fujisaki, H. Path Ensembles for Pin1-Catalyzed Cis-Trans Isomerization of a Substrate Calculated by Weighted Ensemble Simulations. *J. Chem. Theory Comput.* **2021**, *17*, 2522–2529.

(60) Vöhringer-Martinez, E.; Verstraelen, T.; Ayers, P. W. The influence of Ser-154, Cys-113, and the phosphorylated threonine residue on the catalytic reaction mechanism of pin1. *J. Phys. Chem. B* **2014**, *118*, 9871–9880.

Graphical TOC Entry